Multicentury tree ring reconstruction of annual streamflow for the Maule River watershed in south central Chile

Rocío B. Urrutia,[1,2,3] Antonio Lara,[1,2] Ricardo Villalba,[4] Duncan A. Christie,[1] Carlos Le Quesne,[1] and Augusto Cuq[1]

[1]   Because of the reported decreasing trends in precipitation in south central Chile and the high priority of the Valdivian rain forest ecoregion conservation, it is essential to understand long-term changes in water availability in this area. Thus, this study presents a 410 year annual streamflow reconstruction for the Maule River watershed located in a Mediterranean-type climate in the northern part of the ecoregion (35°S–36°30′S). The annual streamflow reconstruction used *Austrocedrus chilensis* tree ring chronologies, and the adjusted R^2 was 0.42. The reconstruction was characterized by interannual, interdecadal, and multidecadal oscillation modes, some of which might be explained by solar and lunar cycles and by ocean-atmospheric forcings. Temporal correlations between the reconstruction and climatic indices, such as the El Niño–Southern Oscillation and the Antarctic Oscillation, demonstrate that water availability is influenced by tropical and high-latitude forcings in this area. Extreme low and high streamflows are particularly related to ocean-atmospheric conditions in the tropical Pacific. The Maule River watershed streamflow reconstruction reveals a higher proportion of streamflows below the mean in the last century compared to the previous three centuries.

1. Introduction

[2]   Water availability has been recognized as one of the main limitations for future economic development for extensive regions of the world [*Arnell et al.*, 2001; *Viviroli et al.*, 2003]. Water resources in south central Chile (35°S–38°S) constitute the foundation of Chile's agricultural and industrial activities, supply drinking water to more than half of the Chilean population, and represent roughly 70% of the country's installed hydropower capacity [*Direccion General de Aguas*, 1999, *Rubio-Álvarez and McPhee*, 2010]. This region, as with other Mediterranean-type climate regions of the world, is an area where both human population and agricultural production are concentrated (with 62% of the total population of the country) and where the competition for water is among the highest in the world [*Gasith and Resh*, 1999; *Instituto Nacional de Estadísticas*, 2009].

[3]   South central Chile constitutes the northern portion of the Valdivian rain forest ecoregion of Chile and adjacent areas of Argentina (35°S–48°S) [*Dinerstein et al.*, 1995;

Lara et al., 2003]. The climate ranges from a Mediterranean-type in the north (35°S–38°S) to a rainy temperate climate south of 40°S [*Miller*, 1976; *Pezoa*, 2003]. This ecoregion is especially important since it represents the main area of temperate forests in South America, and it has been recognized as being one of the most threatened ecosystems in the world by the Global Initiative 200 [*Olson and Dinerstein*, 2002]. This is because of the high level of endemism, threats resulting from anthropogenic activities and climate change [*Villagrán and Hinojosa*, 1997; *Myers et al.*, 2000; *Echeverría et al.*, 2006; *Rodriguez-Cabal et al.*, 2008].

[4]   Streamflow in south central Chile is principally controlled by precipitation under rain-fed or mixed rainfall and snow–dominated regimes [*Niemeyer and Cereceda*, 1984]. Instrumental precipitation records from meteorological stations located between 37°S and 46°S show a decreasing trend since 1931 [*Lara et al.*, 2003; *Pezoa*, 2003], and the south central part of the country has experienced a decrease in precipitation of between 40% and 60% in the period 1901–2005 [*Trenberth et al.*, 2007]. Environmental changes related to the local hydroclimate, such as an increase in the elevation of the 0°C isotherm [*Carrasco et al.*, 2008] and sustained glacier retreat [*Masiokas et al.*, 2009], have also occurred during the last century. Furthermore, increased water demands over recent decades have intensified the problems with water availability [*Lara et al.*, 2003, *Gligo*, 2006]. Finally, central Chile has been identified as one of the key hot spots in Latin America with respect to future climate change because of a reduction in water availability,

---

[1]Laboratorio de Dendrocronología, Instituto de Silvicultura, Facultad de Ciencias Forestales y Recursos Naturales, Universidad Austral de Chile, Valdivia, Chile.
[2]Fundación FORECOS, Valdivia, Chile.
[3]Now at Environmental Change Institute, School of Geography and the Environment, University of Oxford, Oxford, UK.
[4]Departamento de Dendrocronología e Historia Ambiental, Instituto Argentino de Nivología, Glaciología y Ciencias Ambientales, CONICET, Mendoza, Argentina.

growing hydropower demand, and increasing desertification and aridity [*Magrin et al.*, 2007].

[5] Within this context, and to better understand climate variability in south central Chile, it is crucial to assess precipitation and streamflow variability from a long-term perspective of centennial or millennial time scales. This longer perspective permits us to address to what extent the recent trends constitute components of long-term variability in the regional hydroclimate [*Axelson et al.*, 2009].

[6] Tree rings provide annual records, which serve as a commonly used proxy for reconstructing past climate variability. Long-term streamflow reconstructions can be developed by taking advantage of a strong correlation between tree growth series and river discharge. As tree growth responds to climatic variables such as precipitation, and precipitation has a strong regional effect on streamflows, then it is possible to capture discharge variations using the width of tree rings. A number of streamflow reconstructions have been developed for North America [e.g., *Stockton and Jacoby*, 1976; *Meko et al.*, 1995; *Hidalgo et al.*, 2000; *Woodhouse*, 2001; *Brito-Castillo et al.*, 2003; *Woodhouse et al.*, 2006; *Woodhouse and Lukas*, 2006; *Meko et al.*, 2007; *Axelson et al.*, 2009], but only a few have been developed in South America, two of them in Argentina [*Holmes et al.*, 1979; *Cobos and Boninsegna*, 1983] and only one in Chile [*Lara et al.*, 2008]. *Holmes et al.* [1979] reconstructed the streamflow of Limay and Neuquén Rivers in northern Argentinean Patagonia back to 1601 using *Araucaria araucana* (Araucaria) and *Austrocedrus chilensis* (Ciprés de la Cordillera) tree rings, and *Cobos and Boninsegna* [1983] used *Austrocedrus* tree rings from central Chile to reconstruct the streamflow for the Atuel River in Argentina back to 1576.

[7] In the case of Chile the only existing streamflow reconstruction was developed for the Puelo River [*Lara et al.*, 2008], a watershed shared with Argentina, located toward the southern portion of the Valdivian ecoregion (41°35′S). The regional climate in this area is classified as oceanic wet temperate with Mediterranean influence [*Lara et al.*, 2008], and the 400 year reconstruction was developed using *A. chilensis* from northern Argentinean Patagonia and *Pilgerodendrum uviferum* (Ciprés de las Guaitecas) from southern Chile. This reconstruction, which highlighted the low-frequency variability (decadal-interdecadal variability), demonstrated that the decreasing trend in streamflow in the last 2 decades was part of a 84 year cycle that has been intensifying over time and that the river has been strongly influenced by the Antarctic Oscillation in its variability and trend.

[8] Toward the north in the Mediterranean-temperate transition (MTT) zone (37°S–39.5°S), a recent high-frequency reconstruction of the late spring–early summer Palmer drought severity index (PDSI), demonstrated an unprecedented increase in severe and extreme drought events during the last century in the context of the previous six. These events appeared to be linked to tropical (El Niño–Southern Oscillation (ENSO)) and especially to high-latitude (Antarctic Oscillation (AAO)) ocean-atmospheric forcings [*Christie et al.*, 2011].

[9] Given the existing streamflow reconstruction for the Puelo River in the southern part of the Valdivian ecoregion with an oceanic wet temperate climate and the PDSI tree ring record for the MTT zone, it is highly relevant to reconstruct streamflow for the northern portion of the ecoregion under a Mediterranean-type climate. These three reconstructions covering a north-south hydroclimatic gradient can help in understanding the spatial influence of ocean-atmospheric forcings along this transect and might constitute the beginning of a long-term hydroclimatic network.

[10] The main objective of this study was to develop a multicentury low-frequency streamflow reconstruction for this area under a highly variable Mediterranean-type climate in the northern part of the Valdivian rain forest ecoregion, specifically for the Maule River watershed (35°S–36°30′S). The specific objectives were (1) to recognize the most relevant modes of temporal variability in the streamflow reconstruction to better understand the main cycles that characterize streamflow variability in the Mediterranean portion of the ecoregion, (2) to assess changes in variability during the last century compared to the previous centuries, (3) to compare this reconstruction with previous tree ring streamflow and precipitation records in the ecoregion and farther north, and (4) to assess the influence of tropical and high-latitude ocean-atmospheric forcings on hydroclimate in this region and to understand their influence along a north-south gradient in Chile.

2. Methodology

2.1. Study Area

[11] The study area corresponds to the Maule watershed in south central Chile (35°S–36°30′S), covering an area of 21,060 km^2 (Figure 1). The main land cover in the watershed is agricultural lands and pasture (35.7%), shrubland (18%), native forests (14.2%), plantations (11%), and bare land (9%) [*Corporacion Nacional Forestal, Comision Nacional del Medio Ambiente, and Banco Internacional de Reconstruccion y Fomento*, 1999]. Climate in this area is of the Mediterranean type. Annual precipitation varies between approximately 830 mm in the coastal area at the Nirivilo station (35°31′S–72°04′W) and approximately 2300 mm at the Armerillo station (35°42′S–71°04′W) in the Andes. Rain is concentrated in the austral fall and winter (April–August), when over 75% of the annual precipitation occurs [*Miller*, 1976]. According to the available records, the mean temperature is 19°C for January (the warmest month) and 7.9°C for July (the coldest month) at Ancoa at the El Embalse weather station (35°54′S–71°17′W, 430 m above sea level, Dirección General de Aguas (DGA)).

[12] Climate variability in the Maule area is driven by both low- and high-latitude climatic forcings. Extreme dry and wet years are related to the El Niño–Southern Oscillation, where warm ENSO events are characterized by abundant rainfall in winter [*Aceituno*, 1988]. This abundant precipitation produces higher than average streamflows in this season in central Chile (in some cases floods) and higher streamflows in spring and summer due to snowmelt [*Aceituno*, 1992; *Caviedes*, 1998; *Masiokas et al.*, 2010]. In addition, storms in central Chile during El Niño episodes are associated with enhanced blocking activity over the Bellingshausen Sea (90°8′W) that contributes to a northward shift of the storm track in the SE Pacific [*Montecinos and Aceituno*, 2003]. In the case of la Niña, dry conditions with streamflows below the mean characterize central Chile, creating severe restrictions on water supply and irrigation
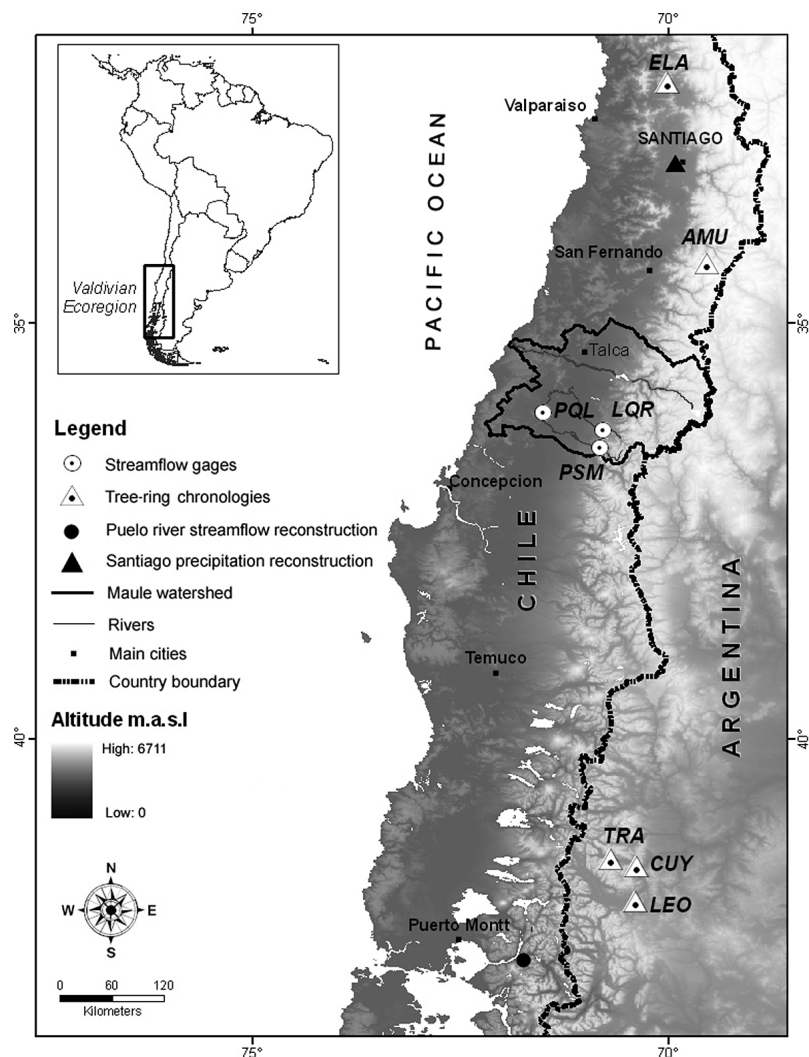
Figure 1. Location of the Maule watershed, the gauging stations, and the tree ring chronologies used to develop the streamflow reconstruction. The Valdivian rain forest ecoregion is also shown. Streamflow record PQL corresponds to Perquilauquén in Quella, PSM corresponds to Perquilauquén in San Manuel, and LQR corresponds to Longaví in La Quiriquina. Codes for chronologies are provided in Table 2. The location of the two tree ring records that were compared to the Maule River streamflow reconstruction is also included (Santiago precipitation and Puelo River streamflow reconstructions).

demands between 25°S and 40°S [*Rutllant and Fuenzalida*, 1991; *NC-Chile*, 1999].

[13] The Antarctic Oscillation also influences climate, and specifically precipitation in this area [*Quintana*, 2004]. The Antarctic Oscillation index is the leading principal component of 850 hPa geopotential height anomalies south of 20°S [*Thompson and Wallace*, 2000]. Positive values in this index are associated with decreased geopotential height over Antarctica and increased geopotential height over midlatitudes (dry conditions over this area).The poleward shift of the storm track and the strengthening of the polar vortex characterize this stage. The reverse conditions are observed during the negative phase of the AAO [*Thompson and Wallace*, 2000].

[14] Finally, it is important to note that precipitation records over South America also display decadal and interdecadal variability, with the most likely forcing behind these fluctuations being the Pacific Decadal Oscillation (PDO) [*Garreaud et al.*, 2009]. The PDO index is defined as the leading principal component of the North Pacific (north of 20°N) monthly sea surface temperatures (SST) variability, and its climate anomalies over South America have been described as ENSO-like [*Garreaud et al.*, 2009]. This means that its warm and cold phases have a strong similarity to those of the El Niño and La Niña events, respectively [*Garreaud and Battisti*, 1999; *Garreaud et al.*, 2009].

2.2. Streamflow Records

[15] Eight streamflow records from the Maule watershed were obtained from the Dirección General de Aguas. The records were previously homogenized, validated, and completed for any missing data by *Rubio-Álvarez and McPhee* [2010]. Streamflow records were completed and validated for homogeneity using the double-mass curve method. Only stations with complete or near-complete records were used in computing the streamflow index for the double-mass

Table 1. Characteristics of the Streamflow Gauges Used in This Study[a]

Streamflow Gauges	Latitude	Longitude	Period	Mean Annual Streamflow (m^3/s)	Standard Deviation	Skewness	First-Order Autocorrelation
PSM	36°25′S	71°30′W	1938–2003	36	14.7	0.68	0.184
LQR	36°14′S	71°28′W	1943–2003	47	16.1	0.16	−0.123
PQL	36°03′S	72°05′W	1963–2003	58	25.1	0.46	−0.125

[a]Complete names are given in the caption of Figure 1.

curve, and cross checking between the index and individual stations was performed in order to keep only those records deemed consistent among each other. Gaps in monthly data were filled by a combination of annual flow correlations and monthly distribution coefficients differentiated by wet, normal, and dry water years [*Rubio-Álvarez and McPhee*, 2010]. Streamflow gauges affected by hydropower generation activities were excluded from the analysis.

[16] The hydrological year for the Maule watershed streamflow spans from April of the current year to March of the following year [*Niemeyer and Cereceda*, 1984]. Maule River annual mean streamflow is approximately 200 m^3/s at the gauge called Maule in Longitudinal (35°34′S–71°43′W).

[17] To obtain suitable streamflow data for the reconstruction, monthly streamflow values of the stations were divided by the mean of the 1965–2000 period; hence, a percentage (%/100) was calculated for every month and for each station. This procedure made all the stations comparably independent of the absolute streamflow values. Monthly and annual plots and correlations between stations were obtained for all the gauges. On the basis of these results, only stations with significant correlations ($p < 0.05$) between each other every month, and with no anomalous patterns in monthly plots (unexplained outliers), were selected as candidate records for use in the reconstruction. The aim was to have the most reliable instrumental records from the selected gauges in order to maximize the regional streamflow signal.

[18] The three gauges that were selected to develop the streamflow reconstruction in the Maule watershed were Perquilauquén in San Manuel (PSM, 36°25′S–71°30′W), Longaví in La Quiriquina (LQR, 36°14′S–71°28′W), and Perquilauquén in Quella (PQL, 36°03′S–72°05′W) (Figure 1 and Table 1). The precipitation and hydrological regime for the three selected stations in the Maule watershed reveal that the streamflow regime of the PQL, the station located farthest from the Andes Cordillera, was clearly rainfall dominated with the major peak of precipitation in winter (June–July). In the case of PSM and LQR (located closer to the Andes), they show a mixed regime with a secondary peak corresponding to snowmelt in the spring. The hydrograph for LQR is shown as an example in Figure 2.

[19] These three stations are located on tributaries of the Maule River since those located along the main reach were incomplete and were affected by the hydropower production. The selected stations represent between 18% and 29% of the annual flow at Maule River, and the correlation between the mean annual streamflow of the three selected gauges and the Maule station on the main reach of the river, Maule in Longitudinal, was 0.87 (1962–2003 period). This indicates that the three selected stations were representative of the streamflow in the watershed. The average of the three streamflow records (mean watershed record) was evaluated

with tree ring data to determine the most appropriate months or seasons for a streamflow reconstruction.

2.3. Tree Ring Chronologies

[20] The tree species selected to develop the Maule watershed streamflow reconstruction was *A. chilensis*. This species grows mainly on the steep topography of the Andean Cordillera of Chile between 32°39′S and 38°S along the western slope of the Andes and between 37°07′ and 43°44′S along the eastern slope of the Andes in Argentina. The climate in these areas is characterized by winter precipitation and dry summers [*Donoso*, 2006]. The growth of *Austrocedrus* is particularly sensitive to precipitation, and individuals can live more than 1200 years [*Le Quesne et al.*, 2006].

[21] Increment cores from living trees and cross sections from dead trees were collected from two *A. chilensis* stands in central Chile and three stands in Argentinean Patagonia (Figure 1). Increment cores from living trees and cross sections were sanded, and tree rings were measured to the 0.001 mm level. Cross dating of the tree ring series was visual and was verified using the computer program COFECHA [*Holmes*, 1983]. For dating purposes, the Schulman convention [*Schulman*, 1956] was followed for the Southern Hemisphere, which assigns to each tree ring the date of the year in which radial growth started. Two of the three chronologies from northern Patagonia were grouped into one composite chronology because of their proximity and high correlation coefficient ($r = 0.49$, 1550–2000, $p < 0.05$).
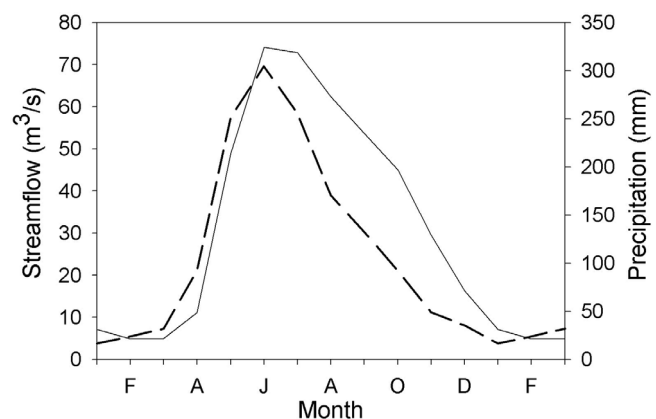

Figure 2. Mean monthly variations of streamflow (solid line) at Longaví in La Quiriquina as an average for the 1938–2004 period. Mean monthly variations of precipitation (dashed line) correspond to Digua in El Embalse, the station close to this streamflow gauge.

Table 2. Characteristics of the Tree Ring Chronologies Used in This Study

Chronologies	Code	Location	Elevation (m)	Number of Series	Period[a]	Correlations[b]
El Asiento	ELA	32°39′S–70°49′W	1700–1900	115	1285–2000	0.50
Agua de la Muerte	AMU	34°31′S–70°25′W	1700–2000	100	1130–2001	0.41
Traful-Cuyín Manzano	TRA-CUY	40°39′S–71°24′W	1000	92	1590–2003	0.47
Cerro Los Leones	LEO	41°05′S–71°09′W	1020	82	1564–2003	0.53

[a]EPS value >0.85.
[b]Significant correlations between each tree ring chronology and annual (April–March) Maule streamflow over the 1938–2000 period.

[22] Ring width measurements for each sample were standardized and averaged to produce a mean stand chronology for each site [*Fritts*, 1976; *Cook*, 1985]. Standardization involves fitting the observed ring width series with a theoretical curve and computing an index of the observed ring widths in relation to the expected value [*Fritts*, 1976]. The standardization was performed using conventional methods in dendrochronology that fit to every individual tree ring series a negative exponential curve or a linear regression. The purpose of the standardization was to remove variability in the tree ring series that was not related to climate (e.g., tree aging or forest disturbances) [*Fritts*, 1976]. This particular method helps to preserve a large percentage of the low-frequency variability, and it was carried out using the ARSTAN software [*Cook*, 1985]. In addition, the variance of the chronologies was stabilized using the method described by *Osborn et al.* [1997]. The site characteristics for each tree ring chronology are described in Table 2.

[23] To evaluate the quality of the tree ring standard chronologies, the expressed population signal (EPS) statistic was calculated for each chronology [*Briffa*, 1995]. EPS is a measure of the similarity between a chronology and a hypothetical chronology that has been infinitely replicated [*Briffa*, 1995]. When the EPS value of the chronology is above a determined threshold (0.85), the chronology can be considered robust, and it is an indication of temporal stability, good quality, and a strong common signal [*Wigley et al.*, 1984]. This statistic is particularly important as the number of samples in a chronology decreases with progression into the past.

[24] It is important to mention that these tree ring chronologies were selected for the reconstruction because of their correlation with streamflow data. These chronologies were chosen from a pool of 19 *Austrocedrus* tree ring chronologies located in Chile and Argentina (between 32°S and 42°S), including nine within the Maule watershed. Chronologies within the watershed did not strongly correlate with the Maule streamflow, probably because these sites appeared to be affected by fires.

2.4. Streamflow Reconstruction

[25] Since the northern, as well as the southern, chronologies were significantly correlated with each other, a principal component analysis of the four chronologies was developed. Hence, the intercorrelated set of chronologies (predictors) was converted to orthogonal variables to reduce the dimension of the regression analysis by removing the eigenvectors that explain a small proportion of the variance [*Cooley and Lohnes*, 1971]. Only eigenvectors with eigenvalues greater than 1 were retained in the model.

[26] The reconstruction equation was estimated by regressing the best correlated seasonal streamflow discharge on the two principal components obtained from the four standard tree ring chronologies. The complete observation period (1938–2000), common to both tree ring and streamflow data, was used for calibration. The leave-one-out cross-validation method was used to validate the regression model [*Michaelsen*, 1987]. In this method a model is calibrated on all values but one, this value is then estimated, and the process is repeated until each value in the calibration period has undergone this process [*Woodhouse and Lukas*, 2006]. The strength of the regression model was characterized by the adjusted R^2 and F level of the equation [*Woodhouse et al.*, 2006], and the ability of the model to reconstruct streamflow variations was assessed using the reduction of error statistic (RE) and the root-mean-square error (RMSE).

[27] To measure the common variance as a function of frequency between the instrumental and reconstructed streamflow, a coherence spectral analysis was conducted [*Jenkins and Watts*, 1968]. The exceedance probability [*Searcy*, 1959], was used to determine changes in variability and in the proportion of extreme years between streamflow during the 20th century and during the previous three centuries.

[28] A continuous wavelet transform analysis was developed to allow a simultaneous representation of the dominant spectral modes of variability in the reconstruction and their variations and significances through time [*Torrence and Compo*, 1998]. The reconstruction was compared to the Santiago annual tree ring precipitation record located north of the ecoregion (33°S) [*Le Quesne et al.*, 2009] (Figure 1) and with the Puelo River summer-fall streamflow reconstruction in the southern portion of the ecoregion (41°35′S) [*Lara et al.*, 2008] (Figure 1). The PDSI reconstruction [*Christie et al.*, 2011], located between the Maule and the Puelo River watersheds, was not considered for comparison because it is a high-frequency reconstruction and does not contain significant cycles at decadal or longer time scales. The comparison was made through a cross-wavelet transform (XWT) that allows determining regions in time frequency space where the selected time series show high common power [*Grinsted et al.*, 2004].

[29] As climate in the Maule region is influenced by low- and high-latitude forcings, Pearson's temporal correlation coefficients between the annual reconstruction and indices of atmospheric circulation were calculated. ENSO, expressed as the El Niño 3.4 index (http://gcmd.nasa.gov/records/GCMD_NOAA_NWS_CPC_NINO34.html), and the Antarctic Oscillation (http://www.ifm-geomar.de/index.php?id=SAM) [*Visbeck*, 2009] were evaluated to identify the major
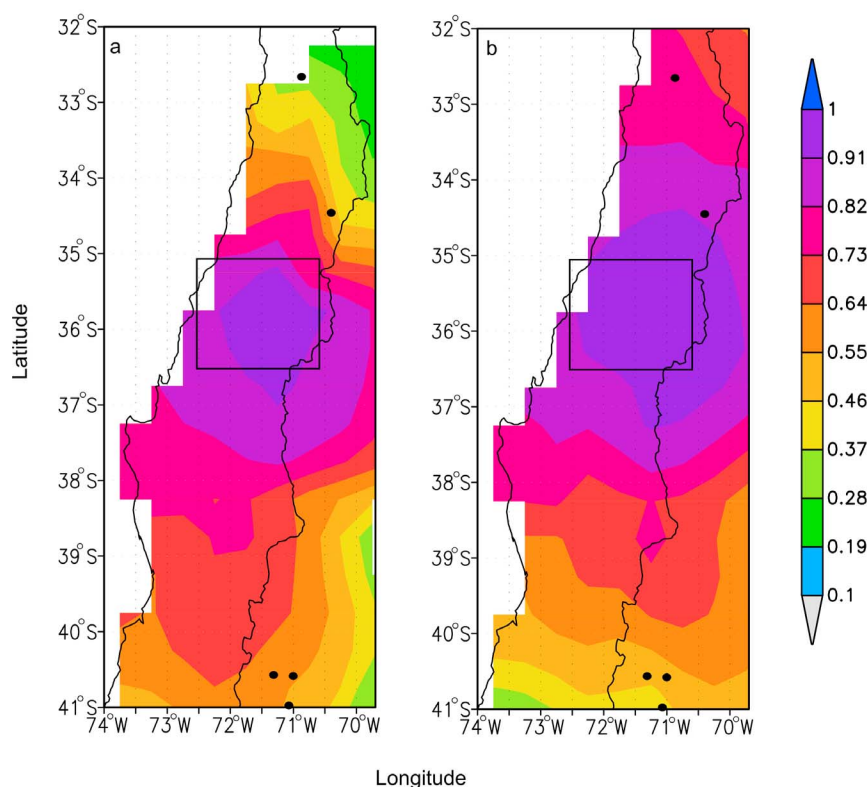
Figure 3. (a) Spatial correlation map of observed summer precipitation (December–March) in the Maule watershed (35°S–36°30′S) and precipitation across a latitudinal range (32°S–41°S). (b) Same as Figure 3a but for winter precipitation (May–August). The period of analysis was 1901–2005, and the map was constructed using the routines available at the Royal Netherlands Meteorological Institute (http://climexp. knmi.nl/select.cgi). The Maule watershed is delimited by the black square, and chronologies are represented by dots.

climatic forcings affecting interannual variations in the Maule watershed discharge. Correlations were assessed after the red noise was removed from the reconstruction and the ENSO and AAO time series, by prewhitening using an autoregressive model where the order was estimated by means of the Akaike information criterion AIC [*Akaike*, 1974]. Using autocorrelated series in this analysis would make the statistical tests of correlation significance too liberal (i.e., too frequent rejection of the null hypothesis, $r = 0$) [*Masiokas et al.*, 2006]. Prewhitening of the time series prevents the adjustment of degrees of freedom for the serial persistence seen in the original data to properly test correlation significance [e.g., *Dawdy and Matalas*, 1964]. Correlations using a 20 year moving window were also calculated between the reconstruction and these two indices.

[30] Finally, to assess the spatial SST pattern that characterized the highest and lowest values of the Maule River streamflow, we selected the 10 lowest and the 10 highest streamflows from the reconstruction within the 1948–2000 period. Two composite anomaly maps were created using gridded (2° × 2°) annual SST series from the NOAA extended reconstructed SST V3b (*Smith and Reynolds* [2003] and updates). These maps were generated using the monthly or seasonal composites and mapping routines available at the Climate Diagnostics Center, National Oceanic and Atmo-

spheric Administration Web site (http://www.esrl.noaa.gov/ psd/cgi-bin/data/composites/printpage.pl).

3. Results

[31] Correlations between the ring width indices of the northern chronologies (Agua de la Muerte and El Asiento) and monthly mean streamflow discharges indicate that the highest significant correlations were during winter and spring (from June to October). In the case of the southern chronologies (Traful-Cuyín Manzano and Cerro Los Leones), the highest significant correlations between tree ring width and monthly streamflow were found in summer (December–March) of the previous growing season and winter (May–August) and spring–summer of the current growing season (November–January). These somewhat dissimilar correlation functions indicate that northern and southern chronologies, and hence tree growth, are related to different seasons of the hydrological cycle, which together allow the reconstruction of a broader period (annual streamflow). Northern chronologies would be capturing winter–spring hydrological information, while southern chronologies would be mostly capturing spring and summer hydrological information. These correlation functions could be explained by winter precipitation in the Maule River watershed being more significantly correlated with winter precipitation in
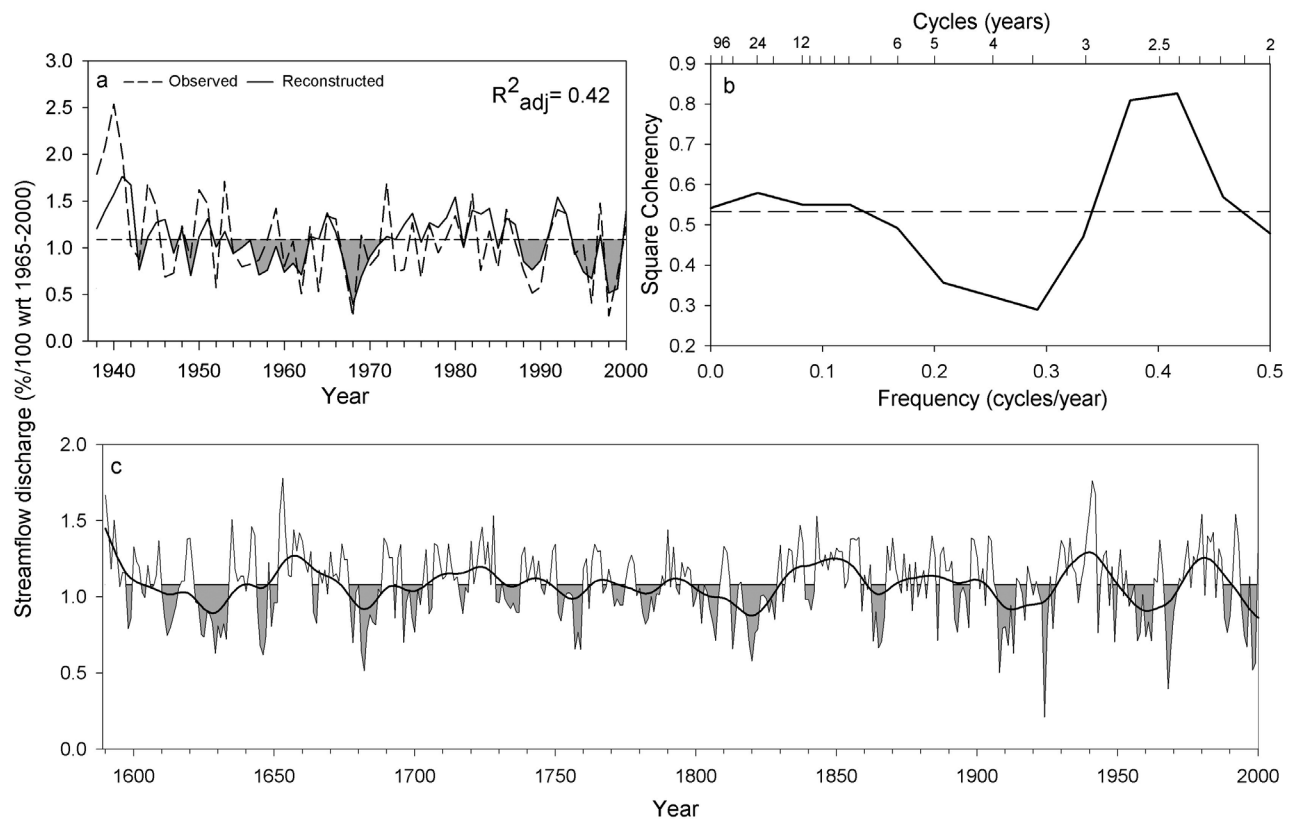
Figure 4. (a) Observed and reconstructed mean annual (April–March) streamflow discharges for the Maule watershed streamflow from 1938 to 2000 expressed in %/100 of average. (b) Coherency spectrum of the observed and reconstructed annual streamflow in the Maule River watershed, estimated over the 1938–2000 period (dashed line indicates the 0.05 probability level). (c) Annual streamflow reconstruction (April–March) of the Maule watershed for the period 1590–2000 represented as discharge (%/100 of average). To emphasize the long-term variations, a cubic spline version designed to reduce 50% of the variance in a sine wave with a periodicity of 25 years is also shown [*Cook and Peters*, 1981].
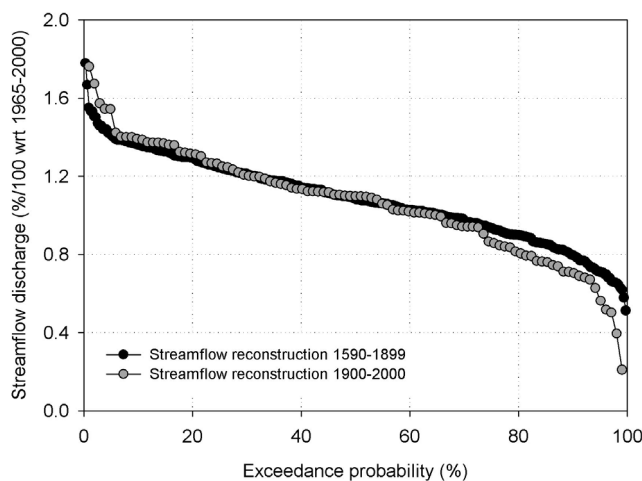

Figure 5. Exceedance probability of the April–March streamflow reconstruction during the period 1590–1899 (black dots) and during the 20th century (gray dots). Streamflow is expressed in %/100 of average.
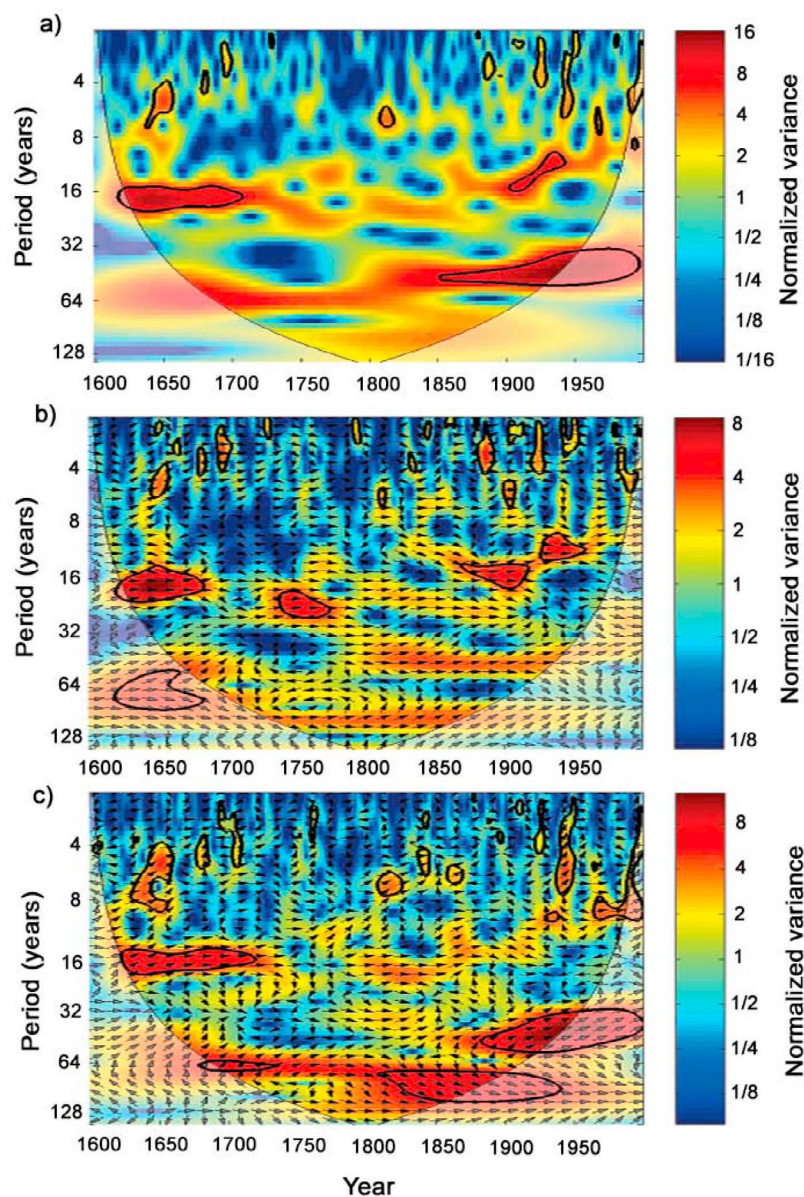
Table 3. List of the Five Highest and Lowest Annual Streamflow Years and Periods Reconstructed for the Maule Watershed Since 1590[a]

Period	Highest Streamflows		Lowest Streamflows	
	Years	Mean Discharge (%/100)	Years	Mean Discharge (%/100)
1	1653	1.779	1924[b]	0.209
	1941	1.761	1968[b]	0.396
	1942[b]	1.674	1908[b]	0.503
	1590	1.667	1682	0.513
	1940[c]	1.573	1998[b,c]	0.518
5	1938–1942[c]	1.523	1818–1822[c]	0.735
	1590–1594	1.418	1908–1912[c]	0.745
	1652–1656	1.405	1628–1632	0.765
	1980–1984	1.347	1682–1686[c]	0.765
	1656–1660	1.332	1966–1970	0.798
10	1650–1659	1.310	1625–1634	0.822
	1975–1984	1.298	1815–1824	0.878
	1935–1944	1.271	1905–1914	0.896
	1720–1729	1.261	1960–1969	0.896
	1850–1859	1.251	1680–1689	0.900

[a]Values are in %/100 of the 1965–2000 mean. The period is given in number of years.

[b]Indicates correspondence with the driest and wettest years found in the 800 year central Chile precipitation reconstruction [*Le Quesne et al.*, 2006].

[c]Indicates correspondence with the highest and lowest streamflows found in the Puelo River streamflow reconstruction [*Lara et al.*, 2008]. Correspondence is close but not exact in the 5 year lowest streamflow periods.

Figure 6. (a) Wavelet power spectrum (Morlet) of the Maule watershed streamflow reconstruction (1590–2000). Thick black contours indicate the 95% significance level using the red noise model, and the cone of influence is shown in lighter and more opaque colors. Cross-wavelet transform between the Maule streamflow reconstruction and (b) the Santiago precipitation reconstruction and (c) the Puelo River streamflow reconstruction. Vectors indicate the relative phase relationship between the reconstructions (horizontal arrows pointing right and left imply in-phase and antiphase relationships, respectively). All significant sections in the cross-wavelet transforms show in-phase relationships between the reconstructions.

central Chile than with southern areas. Conversely, summer precipitation in the Maule River watershed was more significantly correlated with summer precipitation in northern Patagonia than with central Chile (Figure 3).

[32] The first and second principal components (PC1 and PC2) from the four standard tree ring records included the southern and northern chronologies, respectively, contributing with an accumulated explained variance of 79%. Both factor scores were used in the regression equation to reconstruct the mean annual streamflow discharge corresponding to the hydrological year of the Maule River

(April–March; see Table 2 for correlations between chronologies and this annual streamflow).

[33] The final relationship between the annual streamflow discharge as a function of tree rings determined by regression analysis was as follows:

$$SFD_t = 1.0807 + 0.1474(PC1_t) + 0.1797(PC2_t),$$

where SFD_t is estimated streamflow discharge (%/100 of average) for the hydrological year (April–March of year t), $PC1_t$ is principal component amplitude of the two southern
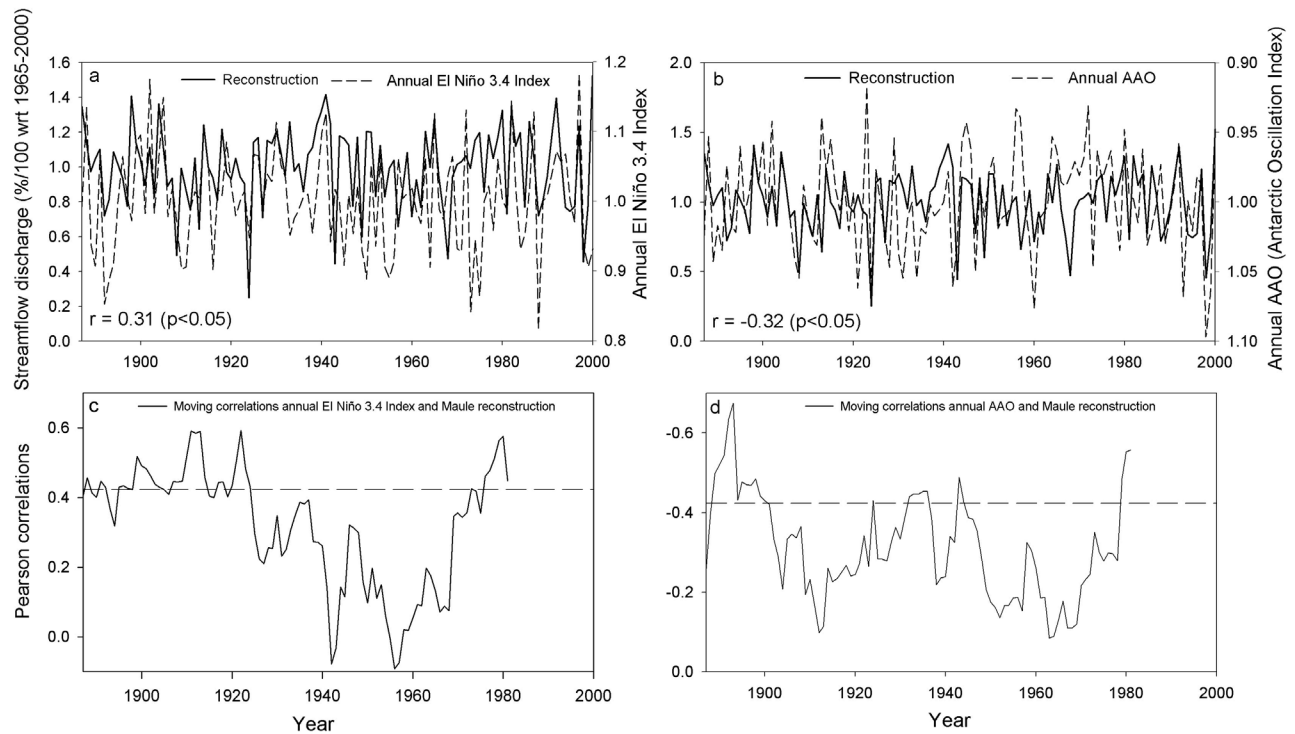
Figure 7. Relationship between the Maule watershed annual streamflow reconstruction and (a) annual El Niño 3.4 index and (b) annual Antarctic Oscillation index for the period 1887–2000. This last index has been inverted to facilitate the comparison with the streamflow data. Correlations between the reconstruction and the mentioned indices are shown. (c) Moving correlations between the Maule annual streamflow reconstruction and annual El Niño 3.4 index. (d) Same as Figure 7c but for the annual AAO. Dashed lines indicate the 0.05 probability level.

chronologies for year t, and $PC2_t$ is principal component amplitude of the two northern chronologies for year t.

[34] The residuals of this regression were normally distributed according to Shapiro-Wilk's W test ($p = 0.321$) and were not significantly autocorrelated according to the Durbin-Watson test (Durbin-Watson statistic of 1.63).

[35] The regression model for the 1938–2000 period was used for the reconstruction of the Maule watershed annual streamflow (April–March), expressed as discharge (%/100 of average), for the interval 1590–2000 (Figure 4c) [*Cook and Peters*, 1981]. The model explained 42% of the total variance in the annual streamflow, and the standard error of the estimate was 0.34. The F value was 22.89. The validation statistic for the model RE was 0.36, a highly positive value indicating useful skill in the regression [*Gordon and Le Duc*, 1981]. Finally, the validation statistic RMSE was 0.35.

[36] The observed and tree ring predicted mean annual (April–March) streamflow for the Maule watershed indicated that below-average streamflow was better reconstructed than above-average streamflow (Figure 4a). This pattern is related to tree ring models being more efficient at predicting restrictive conditions than wet events, and it is probably due to the decreasing sensitivity of tree growth to precipitation above a specific threshold level [*Villalba et al.*, 1998]. This situation is often true in dendrochronological reconstructions of moisture availability, where years of low precipitation match better with tree ring widths than those with high precipitation [*Schulman*, 1956; *Fritts*, 1976; *Sheppard*

et al., 2004; *Gou et al.*, 2007; *Axelson et al.*, 2009; *Gray and McCabe*, 2010]. The two lowest observed and reconstructed annual values in the period with instrumental records were 1968 and 1998 (Figure 4a).

[37] It is important to point out that when the observed and reconstructed streamflows were compared through a coherence spectral analysis, congruence at interannual, decadal, and interdecadal time scales was observed, as revealed by the significant squared coherency at around 2.6, 8, 12, and 24 year cycles. These bandwidths contain the largest proportion of the reconstructed variance (Figure 4b).

[38] In relation to the occurrence of low streamflows in the last century, compared to the previous centuries, the exceedance probability of the reconstructed streamflow for the periods 1590–1899 and 1900–2000 shows that there was a higher proportion of years with streamflow below the mean during the last century compared to the previous three (Figure 5). Moreover, the lowest streamflow in the 20th century was less than half compared to the lowest recorded in the previous three centuries (Table 3). In the case of the extremes of the probability distribution, streamflows were lower or higher in the 1900–2000 period, compared to the 1590–1899 period, demonstrating higher variability in the former. However, it is important to be cautious with high reconstructed streamflows since tree ring series show less ability to capture high compared to low flows. The variances of both distributions were significantly different according to an F test ($p < 0.05$), with values of 0.05 and 0.08, in the previous and last centuries, respectively.
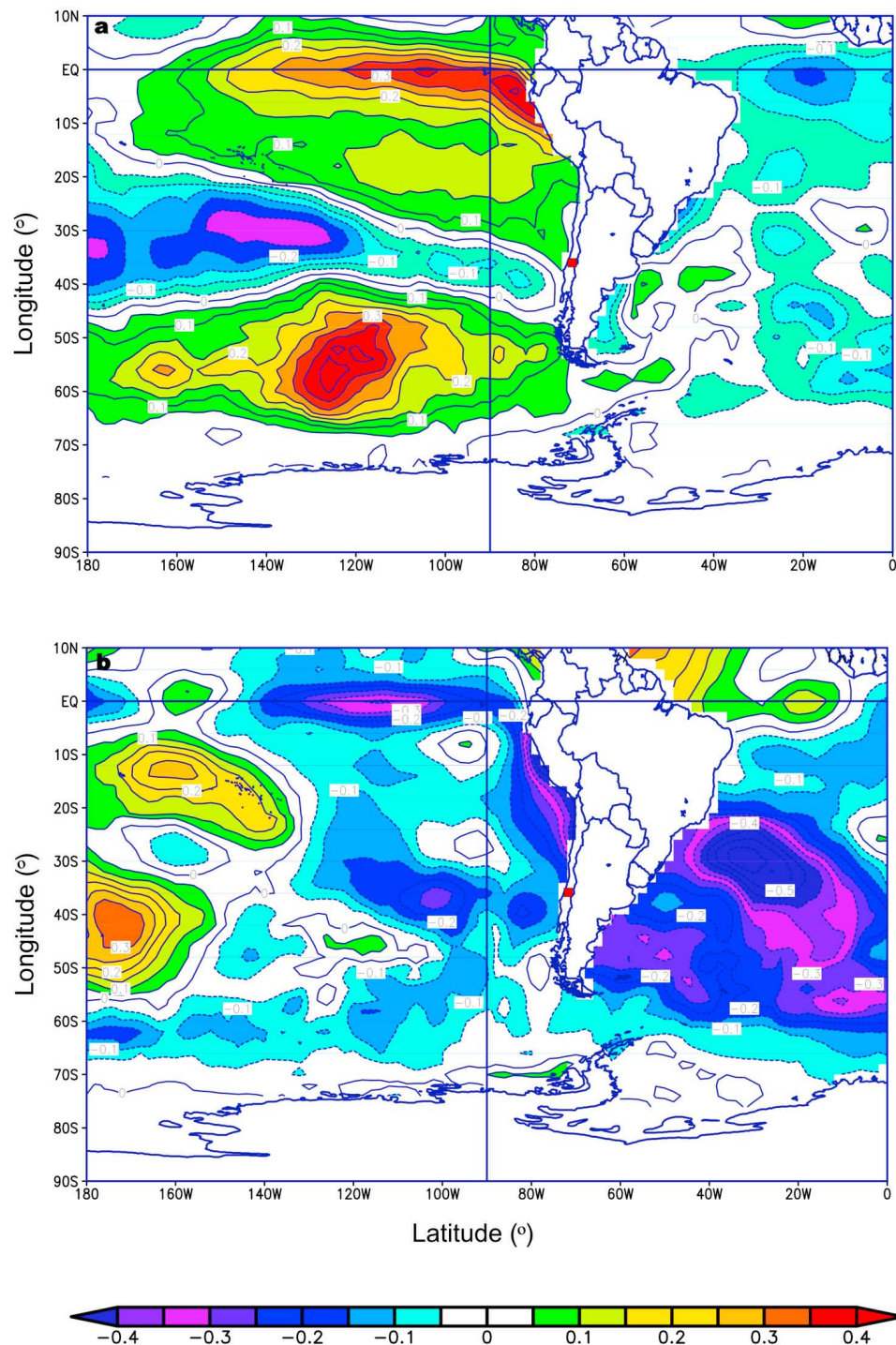
Figure 8. Composite annual SST anomalies from the 1971–2000 mean for (a) the 10 highest and (b) the 10 lowest Maule annual streamflow reconstructed years from the 1948–2000 period. Mean monthly gridded data were obtained from the NOAA extended reconstructed SST V3b (*Smith and Reynolds* [2003] and updates). Positive (negative) contour anomalies are shown as solid (dashed) lines. The red square indicates the location of the Maule River basin.

[39] A list of the lowest and highest streamflows reconstructed for the Maule watershed since 1590 shows that four out of the five lowest annual streamflows occurred during the 20th century, the lowest being in 1924 (Table 3). In relation to the highest-streamflow years, three consecutive years, 1940, 1941, and 1942 were reported in this category in the 20th century. Across the streamflow reconstruction the 5 year lowest streamflow periods were 1818–1822 and 1908–1912, and the two 5 year highest streamflow periods were 1938–1942 and 1590–1594. Two of the five 5 year

lowest and highest streamflow periods were in the 20th century.

[40] In terms of the 10 year moving averages, the period from 1625 to 1634 was ranked driest among the five lowest-streamflow events over the past 410 years, and the period from 1650 to 1659 was ranked at the top of the highest streamflows in the last four centuries. Longer periods with low streamflow values in the reconstruction were 1610–1635, 1800–1830, 1905–1930, 1950–1970, and 1985–2000, three of which were in the 20th century (Figure 4c).

[41] The significant periodicity of the reconstruction across the time frequency domain detected using wavelet power spectrum shows that there is an interdecadal mode close to 18 years that was more prominent up to 1700; it weakened after that and appeared again around 1900 when it changed to a shorter cycle (Figure 6a). According to a singular spectral analysis (results not shown) [*Vautard and Ghil*, 1989], this cycle accounts for 30% of the variance in the reconstruction, clearly explaining a large portion of the Maule River long-term variability. The wavelet power spectrum also shows a 5 to 6 decade mode that appears across the reconstruction, which was significant only from the mid-1800s. Finally, short cycles (i.e., ≤8 years) were more evident in the 17th century and since the end of the 19th century (Figure 6a).

[42] The XWT results reveal that the Maule streamflow reconstruction shows intermittent common spectral power with both the Puelo River streamflow and the Santiago precipitation reconstructions over the last 400 years (Figures 6b and 6c). There is a common power between the Maule and Santiago reconstructions, especially at shorter cycles (<6 years) and between the Maule and Puelo reconstructions at multidecadal cycles (>50 years). The three reconstructions contain common spectral power at a bidecadal scale (approximately 18 years), particularly before 1700 (Figures 6b and 6c).

[43] Correlations between the Maule streamflow reconstruction and El Niño 3.4 and AAO demonstrate that the Maule annual streamflow is significantly correlated with both forcings across the 1887–2000 period (Figures 7a and 7b). The best correlations were obtained with these forcings at their annual rather than seasonal resolution. Correlations were positive with the El Niño 3.4 index, indicating that there is a good correspondence between high tropical SSTs and high streamflows and negative with AAO, indicating that above-average streamflows are significantly related to the negative phase of the Antarctic Oscillation (weakened sea level pressure (SLP) in the midlatitudes and intensified SLP in Antarctica). Furthermore, correlations using a 20 year moving window revealed that Maule streamflow is significantly correlated with both forcings at the end of the 19th century and more significantly correlated with ENSO rather than AAO at the beginning of the 20th century. This condition reverses around the middle of the 20th century, and correlations are again significant with both forcings at the end of the century (Figures 7c and 7d).

[44] Finally, the composite SST anomaly maps of the 10 highest streamflows (1980, 1992, 1984, 1982, 2000, 1965, 1975, 1993, 1983, and 1979) were characterized by a pattern of tropical SST above the mean (1971–2000), typical of El Niño years. On the other hand, the 10 lowest streamflows (1968, 1998, 1999, 1996, 1969, 1949, 1962, 1957, 1960, and 1995) were characterized by tropical sea surface temperatures below the mean, resembling the pattern of La Niña years (Figures 8a and 8b).

4. Discussion and Conclusions

[45] The 410 year annual streamflow reconstruction presented in this paper is the first one for the Mediterranean-type climate in Chile and the second streamflow reconstruction using tree rings in the country. This study is especially useful in understanding the temporal variability of water availability in a Mediterranean area, where conservation is a priority and water is fundamental for ecosystems maintenance and economic activities such as agriculture, hydroelectric power generation, and tourism.

[46] The annual streamflow reconstruction was developed using the first and second principal components of four chronologies located in the north (32°S–34°S) and south (40°S–41°S) of the study area. The fact that chronologies from these two areas were correlated with Maule watershed streamflow means that the precipitation regime in this watershed would be representing a transitional situation between the Mediterranean-type climate existing in central Chile and the temperate climate of northern Patagonia. This transitional regime is supported by the significant and stronger correlation ($r > 0.55$, $p < 0.05$, 1901–2005) between summer precipitation in the Maule River watershed (35°S–36°30′S) and summer precipitation in northern Patagonia, compared to summer precipitation in central Chile, where correlations were not always significant. This is also supported by the significant and stronger correlation ($r > 0.73$, $p < 0.05$, 1901–2005) between winter rainfall in the Maule watershed and precipitation in central Chile, compared to winter precipitation in northern Patagonia ($r < 0.55$, 1901–2005).

[47] The regression model explained 42% of the total variance in the annual (April–March) Maule watershed streamflow, a value that is lower than those obtained for streamflow reconstructions in Argentina (53.3% by *Holmes et al.* [1979] and 50.4% by *Cobos and Boninsegna* [1983]) but the same as that obtained for the Puelo River streamflow reconstruction in Chile [*Lara et al.*, 2008].

[48] The two lowest observed and reconstructed streamflows during the observed period were 1968 and 1998. The year 1968 was the second driest year recorded in Santiago's precipitation after 1924 [*Rutllant and Fuenzalida*, 1991], and 1998 was recorded as the second-lowest summer streamflow in the Puelo River and as one of the 10 driest years in the winter–spring precipitation reconstruction of central Chile for the last 800 years (Table 3) [*Le Quesne et al.*, 2006; *Lara et al.*, 2008].

[49] According to the exceedance probability analysis, the Maule watershed streamflow reconstruction shows a higher proportion of streamflows below the mean in the last century compared to the previous three. Similar findings for a tree ring precipitation record in central Chile and for a PDSI reconstruction in the MTT were reported by *Le Quesne et al.* [2006] and *Christie et al.* [2011], respectively. Both studies found an increase in the recurrence of drought during the last century compared to the previous 600–800 years.

[50] Regarding the highest and lowest streamflows in the reconstruction, 4 of the 5 years with the lowest streamflows in the last 410 years occurred in the 20th century, reinforcing the previous result obtained through the probability exceedance

method that refers to a higher proportion of dry conditions in the last century compared to the previous ones. The lowest streamflow was observed for 1924, which was also the year with the lowest annual precipitation recorded in Santiago [*Ruttlant and Fuenzalida*, 1991]. The four lowest streamflows in the 20th century in this reconstruction (1908, 1924, 1968, and 1998) were also reported as part of the 10 driest years of the 800 year central Chile precipitation reconstruction (Table 3) [*Le Quesne et al.*, 2006], and 1998 was also reported among the 10 driest years in the December PDSI reconstruction for the MTT zone from 1948 to 2002 [*Christie et al.*, 2011].

[51] The years with the highest streamflow in the 20th century reconstruction included 1940, 1941, and 1942. The year 1940 was also reported as one with the highest streamflow in the Puelo River streamflow reconstruction (Table 3) and as one with the highest precipitation in the reconstruction using *Nothofagus pumilio* in the central Andes [*Lara et al.*, 2001]. The year 1941 was also among the wettest years in the central Andes reconstruction and in the northern Patagonian precipitation reconstruction [*Villalba et al.*, 1998]. Finally, the year 1942 was among the 10 wettest years in the June–December precipitation reconstruction for central Chile (Table 3) [*Le Quesne et al.*, 2006]. The common occurrence of wet and dry years in these three different areas implies that in some cases the intensity of the signal is strong enough to cover a broad area. In the case of 1998 it coincides with a reported La Niña event, and in the case of 1940, 1941, and 1942 it coincides with a strong and prolonged El Niño event [*Brönnimann et al.*, 2004; *Gergis and Fowler*, 2009].

[52] Three of the 5 year periods with the lowest streamflows closely match with periods observed in the Puelo River streamflow reconstruction (1679–1683, 1818–1822, and 1910–1914, Table 3); it is important to mention that both reconstructions share only one chronology. The period 1818–1822 also had a close correspondence with the annual precipitation reconstruction for northern Patagonia [*Villalba et al.*, 1998]. In relation to the 5 year highest streamflows, the only period that had a close coincidence with the Puelo River streamflow and the precipitation reconstruction from northern Patagonia is the period from 1938 to 1942 (Table 3).

[53] One of the most important oscillatory modes is the approximately 18 year cycle, which was especially relevant before 1700 and in the 20th century, when it transforms to a shorter cycle. This cycle, which explains a high proportion of the variance (30%), might possibly be related to the lunar tidal 18.6 year cycle. Similar oscillations were also found in the Puelo River streamflow reconstruction (19 years) and in the two *Fitzroya cupressoides* temperature reconstructions in Chile and Argentina (20.5 years) [*Villalba et al.*, 1996]. However, the 22 year Hale solar cycle was invoked to explain these oscillations in the temperature reconstructions [*Villalba et al.*, 1996]. The 18.6 year lunar tidal maxima has been reported to have a statistical association with drought occurrence in the western United States [*Currie*, 1984a, 1984b; *Cook et al.*, 1997], but currently there are no studies of this type for southern South America.

[54] The other oscillatory mode is the 50–60 year cycle, particularly significant after 1850. The 50–60 year cycle might be explained by the half-Gleissberg solar magnetic cycle or possibly by the Pacific Decadal Oscillation (PDO),

with an approximate cycle of around 50 years in a tree ring reconstruction for the past millennium [*MacDonald and Case*, 2005]. According to these authors the 50–70 year cycle that they found was especially strong and significant in the last ~200 years, and this is in agreement with this study. Nevertheless, at internannual time scales the relationship of this reconstruction with the PDO is rather weak ($r = 0.2$ with summer PDO, $p < 0.05$, 1900–2000).

[55] The shortest mode of variability in the reconstruction (<8 years) may correspond to the El Niño–Southern Oscillation recurrence cycle, which has apparently increased in activity over the past 50–100 years [*Vecchi and Wittenberg*, 2010]. This was partially corroborated through a cross-wavelet transform between the reconstruction and annual ENSO (SST in the El Niño 3.4 region), in which a special common power was found at the end of the 19th and 20th centuries (not shown). In addition, the occurrence of this short mode of variability in the 1600s corresponds to strong activity reported for ENSO during this period [*Cobb et al.*, 2003]. Further advanced statistical analyses of any relationship between cycles found in the Maule River streamflow reconstruction and their possible causes are beyond the scope of this paper.

[56] The comparison between the Maule streamflow reconstruction and two hydroclimatic reconstructions to the north and south of this area demonstrates that the Maule streamflow is related to hydroclimatic conditions in both areas. The bidecadal cycle is a common feature across the complete north-south hydroclimatic gradient, especially prior to 1700. In addition, the common power is especially strong at short time scales with the northern record, probably associated with ENSO. This was partially corroborated through cross-wavelet transforms between each reconstruction (Maule and Santiago) and the annual ENSO record (SST in the El Niño 3.4 region, not shown), with both analyses showing a strong common power at these time scales, particularly toward the end of the 19th and 20th centuries.

[57] Regarding the XWT between the Maule and southern reconstructions, the common power is especially strong on multidecadal time scales. These multidecadal oscillations might be associated with solar or ocean-atmospheric forcing cycles (PDO). However, it is important to mention that the strong common power found at short time scales (<8 years) in the mid-20th century could be associated with the AAO, since cross-wavelet transforms between the Maule and the Puelo reconstructions and the annual AAO record (not shown) demonstrated the same spectral signature.

[58] Temporal correlations between the Maule record and climatic forcings at low and high latitudes indicate that, at least during the common observed period (1887–2000), streamflow in this area has been almost equally influenced by climatic features of both regions. However, correlations vary when using a moving correlation window; a stronger influence of ENSO at the beginning of the 20th century emerges compared to the AAO influence. Both ENSO and AAO appear significantly related to Maule streamflow in the last decades. The significant relationship of Maule streamflow with ENSO is in agreement with what was found by *Rubio-Álvarez and McPhee* [2010] for a regional observed streamflow series (between 34°S and 37.5°S).

[59] Toward the north of Maule (central Chile), there is a well-documented climate sensitivity to the equatorial Pacific

conditions [*Escobar and Aceituno*, 1998; *Montecinos and Aceituno*, 2003; *Garreaud et al.*, 2009]. However, toward the south, a much stronger climate sensitivity to high-latitude forcings (AAO) compared to ENSO has been reported. This is the case for the PDSI in the MTT zone [*Christie et al.*, 2011] and for the Puelo River streamflow under an oceanic wet temperate climate [*Lara et al.*, 2008]. This fact further reinforces the idea that climatic conditions in the Maule region, influenced equally by low- and high-latitude climatic forcings, constitute a transitional regime between streamflow and precipitation in central Chile and northern Patagonia.

[60] Finally, it is important to highlight that, although the Maule annual streamflow is significantly related to both ENSO and AAO throughout the observed period (1887–2000), extreme streamflow conditions (the 10 highest and lowest streamflows) exhibit a characteristic ENSO pattern (positive and negative temperature anomalies in the tropical Pacific) rather than an AAO pattern. This indicates that extreme conditions in this region would be related more to tropical ocean-atmospheric conditions rather than high-latitude forcings.

[61] In relation to ENSO, a forcing that has been related to Maule annual streamflow especially in the 1700s and in the last century; future changes in the streamflow associated with this phenomenon are uncertain. The future influence of global warming on ENSO variability is currently not well understood, and predictions of variability vary from a slight increase to no changes or even a decrease [*van Oldenborgh and Collins*, 2005]. *Philip and van Oldenborgh* [2006] mention that different changes expected for atmospheric variables compensate for each other, and the residual change in ENSO appears to be relatively small. In any case, an increase in the ENSO activity would trigger an increase in the interannual variability of precipitation and streamflow in the Maule River watershed.

[62] In relation to the AAO, a forcing related to the Maule streamflow, especially at the end of the 19th century and at the middle and the end of the 20th century, a positive trend in this index has occurred particularly since the mid-1960s [*Marshall*, 2003]. Empirical and modeling studies indicate that this trend is largely related to the decrease in stratospheric ozone and an increase in greenhouse gases [*Thompson and Solomon*, 2002; *Gillett and Thompson*, 2003; *Cai et al.*, 2003; *Marshall et al.*, 2004; *Shindell and Schmidt*, 2004; *Arblaster and Meehl*, 2006]. Predicted changes for the end of the 21st century show that even when the ozone layer recovers in the stratosphere, ever-increasing greenhouse gases will continue the already observed positive trend [*Arblaster and Meehl*, 2006]. This projected trend might bring drier conditions to midlatitudes and might likely have an effect on the Maule watershed streamflow. However, this influence would be weaker than the one reported further south, where there is a stronger correlation between hydro-climatic records and the AAO [*Lara et al.*, 2008].

[63] The present streamflow reconstruction in a Mediterranean-type climate in the northern portion of the Valdivian rain forest ecoregion provides the first reconstructed streamflow record in this area for the 1590–2000 period. This reconstruction illustrating past long-term streamflow variability, its associated oscillatory modes, and its relationships with large-scale climatic forcings provides valuable information for decision makers in water resources planning. This is especially crucial since it is one of the most popu-lated areas of the country with an increased water demand and a sustained decrease in precipitation in the 20th century.

References

Aceituno, P. (1988), On the functioning of the Southern Oscillation in the South American sector. Part I. Surface climate, *Mon. Weather Rev.*, *116*, 505–524, doi:10.1175/1520-0493(1988)116<0505:OTFOTS>2.0.CO;2.

Aceituno, P. (1992), Anomalías de precipitación en Chile central relacionadas con la Oscilación del Sur: Mecanismos asociados, paper presented at Paleo ENSO Records International Symposium, Off. Rech. Sci. et Tech., Lima.

Akaike, H. (1974), A new look at the statistical model identification, *IEEE Trans. Autom. Control*, *19*, 716–723, doi:10.1109/TAC.1974.1100705.

Arblaster, J., and G. Meehl (2006), Contributions of external forcings to Southern Annular Mode trends, *J. Clim.*, *19*, 2896–2905, doi:10.1175/JCLI3774.1.

Arnell, N., C. Liu, R. Compagnucci, L. da Cunha, K. Hanaki, C. Howe, G. Mailu, I. Shiklomanov, and E. Stakhiv (2001), Hydrology and water resources, in *Climate Change 2001: Impacts, Adaptation and Vulnerability*, edited by J. J. McCarthy et al., chap. 4, pp. 193–233, Cambridge Univ. Press, Cambridge, U. K.

Axelson, J. N., D. J. Sauchyn, and J. Barichivich (2009), New reconstructions of streamflow variability in the South Saskatchewan River Basin from a network of tree ring chronologies, Alberta, Canada, *Water Resour. Res.*, *45*, W09422, doi:10.1029/2008WR007639.

Briffa, K. R. (1995), Interpreting high-resolution proxy climate data: The example of dendroclimatology, in *Analysis of Climate Variability: Applications of Statistical Techniques*, edited by H. Von Storch and A. Navarra, pp. 77–94, Springer, Berlin.

Brito-Castillo, L., S. Díaz-Castro, C. A. Salinas-Zavala, and A. V. Douglas (2003), Reconstruction of long-term winter streamflow in the Gulf of California continental watershed, *J. Hydrol.*, *278*, 39–50, doi:10.1016/S0022-1694(03)00131-8.

Brönnimann, S., J. Luterbacher, J. Staehelin, T. M. Svendby, G. Hansen, and T. Svenøe (2004), Extreme climate of the global troposphere and stratosphere in 1940–42 related to El Niño, *Nature*, *431*, 971–974, doi:10.1038/nature02982.

Cai, W., P. H. Whetton, and D. J. Karoly (2003), The response of the Antarctic Oscillation to increasing and stabilized atmospheric CO_2, *J. Clim.*, *16*, 1525–1538, doi:10.1175/1520-0442-16.10.1525.

Carrasco, J. F., R. Osorio, and G. Casassa (2008), Secular trend of the equilibrium-line altitude on the western side of the southern Andes, derived from radiosonde and surface observations, *J. Glaciol.*, *54*, 538–550, doi:10.3189/002214308785837002.

Caviedes, C. (1998), Influencia de ENOS sobre las variaciones interanuales de ciertos ríos en América del Sur, *Bull. Ins. Fr. Etudes Andines*, *27*(3), 627–641.

Christie, D. A., J. A. Boninsegna, M. K. Cleaveland, A. Lara, C. Le Quesne, M. S. Morales, M. Mudelsee, D. W. Stahle, and R. Villalba (2011), Aridity changes in the temperate-Mediterranean transition of the Andes since AD 1346 reconstructed from tree-rings, *Clim. Dyn.*, *36*, 1505–1521, doi:10.1007/s00382-009-0723-4.

Cobb, K. M., C. D. Charles, H. Cheng, and R. L. Edwards (2003), El Niño–Southern Oscillation and tropical Pacific climate during the last millennium, *Nature*, *424*, 271–276, doi:10.1038/nature01779.

Cobos, D. R., and J. A. Boninsegna (1983), Fluctuations of some glaciers in the upper Atuel River basin, Mendoza, Argentina, *Quat. S. Am. Antarct. Peninsula*, *1*, 61–82.

Corporacion Nacional Forestal, Comision Nacional del Medio Ambiente, and Banco Internacional de Reconstruccion y Fomento (1999), Catastro y evaluación de los recursos vegetacionales nativos de Chile, 87 pp., Santiago.

Cook, E. R. (1985), A time series analysis approach to tree-ring standardization, Ph.D. dissertation, Univ. of Ariz., Tucson.

Cook, E. R., and K. Peters (1981), The smoothing spline: A new approach to standardizing forest interior ring-width series for dendroclimatic studies, *Tree Ring Bull.*, *41*, 45–53.

Cook, E. R., D. M. Meko, and C. W. Stockton (1997), A new assessment of possible solar and lunar forcing of the bidecadal drought rhythm in the western United States, *J. Clim.*, *10*, 1343–1356, doi:10.1175/1520-0442(1997)010<1343:ANAOPS>2.0.CO;2.

Cooley, W. W., and P. R. Lohnes (1971), *Multivariate Data Analysis*, John Wiley, New York.

Currie, R. (1984a), Evidence for 18.6-year lunar nodal drought in western North America during the past millennium, *J. Geophys. Res.*, *89*, 1295–1308, doi:10.1029/JD089iD01p01295.

Currie, R. (1984b), Periodic (18.6-year) and cyclic (11-year) induced drought and flood in western North America, *J. Geophys. Res.*, *89*, 7215–7230, doi:10.1029/JD089iD05p07215.

Dawdy, D. R., and N. C. Matalas (1964), Statistical and probability analysis of hydrologic data. Part III. Analysis of variance, covariance, and time series, in *Handbook of Applied Hydrology: A Compendium of Water-Resources Technology*, edited by V. T. Chow, pp. 8.68–8.90, McGraw-Hill, New York.

Dinerstein, E., D. Olson, D. Graham, A. Webster, S. Primm, M. Bookbinder, and G. Ledec (1995), A conservation assessment of the terrestrial eco-regions of Latin America and the Caribbean, 129 pp., World Bank, Washington, D. C.

Direccion General de Aguas (1999), Política nacional de recursos hídricos, 63 pp., Minist. de Obras, Santiago.

Donoso, C. (2006), *Las Especies Arbóreas de los Bosques Templados de Chile y Argentina*, Marisa Cuneo, Valdivia, Chile.

Echeverría, C., D. Coomes, J. Salas, J. M. Rey Benayas, A. Lara, and A. Newton (2006), Rapid deforestation and fragmentation of Chilean temperate forests, *Biol. Conserv.*, *130*, 481–494, doi:10.1016/j.biocon.2006.01.017.

Fritts, H. C. (1976), *Tree Rings and Climate*, 567 pp., Academic, London.

Garreaud, R. D., and D. S. Battisti (1999), Interannual (ENSO) and inter-decadal (ENSO-like) variability in the Southern Hemisphere tropo-spheric circulation, *J. Clim.*, *12*, 2113–2123, doi:10.1175/1520-0442(1999)012<2113:IEAIEL>2.0.CO;2.

Garreaud, R., M. Vuille, R. Compagnucci, and J. Marengo (2009), Present-day South American climate, *Palaeogeogr. Palaeoclimatol. Palaeoecol.*, *281*, 180–195, doi:10.1016/j.palaeo.2007.10.032.

Gasith, A., and V. H. Resh (1999), Streams in Mediterranean climate regions: Abiotic influences and biotic responses to predictable seasonal events, *Annu. Rev. Ecol. Syst.*, *30*, 51–81, doi:10.1146/annurev.ecolsys.30.1.51.

Gergis, J. L., and A. M. Fowler (2009), Multiproxy El Niño–Southern Oscillation (ENSO) event reconstructions, *Data Contrib. Ser. 2009-020*, Natl. Clim. Data Cent., Paleoclimatol. Program, NOAA, Boulder, Colo.

Gillett, N. P., and D. W. J. Thompson (2003), Simulation of recent Southern Hemisphere climate change, *Science*, *302*, 273–275, doi:10.1126/science.1087440.

Gligo, N. (2006), *Informe País: Estado del Medio Ambiente en Chile 2005*, Inst. de Asuntos Públicos, Univ. de Chile, Santiago.

Gordon, G. A., and S. K. Le Duc (1981), Verification statistics for regres-sion models, paper presented at the Seventh Conference on Probability and Statistics in Atmospheric Sciences, Am. Meteorol. Soc., Monterey, Calif.

Gou, X., F. Chen, E. Cook, G. Jacoby, M. Yang, and J. Li (2007), Stream-flow variations of the Yellow River over the past 593 years in western China reconstructed from tree rings, *Water Resour. Res.*, *43*, W06434, doi:10.1029/2006WR005705.

Gray, S. T., and G. J. McCabe (2010), A combined water balance and tree ring approach to understanding the potential hydrologic effects of cli-mate change in the central Rocky Mountain region, *Water Resour. Res.*, *46*, W05513, doi:10.1029/2008WR007650.

Grinsted, A., J. C. Moore, and S. Jevrejeva (2004), Application of the cross wavelet transform and wavelet coherence to geophysical time series, *Nonlinear Processes Geophys.*, *11*, 561–566, doi:10.5194/npg-11-561-2004.

Hidalgo, H. G., T. C. Piechota, and J. A. Dracup (2000), Alternative principal components regression procedures for dendrohydrologic reconstructions, *Water Res.*, *36*(11), 3241–3249, doi:10.1029/2000WR900097.

Holmes, R. L. (1983), Computer-assisted quality control in tree-ring dating and measurements, *Tree Ring Bull.*, *43*, 69–75.

Holmes, R. L., C. W. Stockton, and V. C. LaMarche (1979), Extension of river flow records in Argentina from long tree-ring chronologies, *Water Resour. Bull.*, *15*(4), 1081–1085.

Instituto Nacional de Estadísticas (2009), Estadísticas vitales, informe anual 2007, Santiago.

Jenkins, G. M., and D. G. Watts (1968), *Spectral Analysis and Its Applica-tions*, 525 pp., Holden-Day, San Francisco, Calif.

Lara, A., J. A. Aravena, A. Wolodarsky, R. Villalba, B. Luckman, and R. Wilson (2001), Dendroclimatology of high-elevation *Nothofagus pumilio* forests in the central Andes of Chile, *Can. J. For. Res.*, *31*, 925–936.

Lara, A., D. Soto, J. Armesto, P. Donoso, C. Wernli, L. Nahuelhual, and F. Squeo (Eds.) (2003), *Componentes Científicos Clave Para una Política Nacional Sobre Usos, Servicios y Conservación de los Bosques Nativos Chilenos*, Iniciativa Cient. Milenio de Mideplan, Univ. Austral de Chile, Valdivia, Chile. [Available at http://www.forecos.net/contenido_biblioteca.php.]

Lara, A., R. Villalba, and R. Urrutia (2008), A 400-year tree-ring record of the Puelo River summer–fall streamflow in the Valdivian rainforest ecor-egion, Chile, *Clim. Change*, *86*(3–4), 331–356, doi:10.1007/s10584-007-9287-7.

Le Quesne, C., D. Stahle, M. Cleaveland, M. Therrell, J. A. Aravena, and J. Barichivich (2006), Ancient *Austrocedrus* tree-ring chronologies used to reconstruct central Chile precipitation variability from A.D. 1200 to 2000, *J. Clim.*, *19*, 5731–5744, doi:10.1175/JCLI3935.1.

Le Quesne, C., C. Acuña, J. A. Boninsegna, A. Rivera, and J. Barichivich (2009), Long-term glacier variations in the central Andes of Argentina and Chile, inferred from historical records and tree- ring reconstructed precipitation, *Palaeogeogr. Palaeoclimatol. Palaeoecol.*, *281*, 334–344, doi:10.1016/j.palaeo.2008.01.039.

MacDonald, G., and R. Case (2005), Variations in the Pacific Decadal Oscillation over the past millennium, *Geophys. Res. Lett.*, *32*, L08703, doi:10.1029/2005GL022478.

Magrin, G., C. Gay García, D. Cruz Choque, J. C. Giménez, A. R. Moreno, G. J. Nagy, C. Nobre, and A. Villamizar (2007), Latin America, in *Climate Change 2007: Impacts, Adaptation and Vulnerability. Contribu-tion of Working Group II to the Fourth Assessment Report of the Inter-governmental Panel on Climate Change*, edited by M. L. Parry et al., pp. 581–615, Cambridge Univ. Press, Cambridge, U. K.

Marshall, G. (2003), Trends in the Southern Annular Mode from observations and reanalyses, *J. Clim.*, *16*, 4134–4143, doi:10.1175/1520-0442(2003)016<4134:TITSAM>2.0.CO;2.

Marshall, G. J., P. A. Stott, J. Turner, W. M. Connolley, J. C. King, and T. A. Lachlan-Cope (2004), Causes of exceptional atmospheric circula-tion changes in the Southern Hemisphere, *Geophys. Res. Lett.*, *31*, L14205, doi:10.1029/2004GL019952.

Masiokas, M. H., R. Villalba, B. Luckman, C. Le Quesne, and J. C. Aravena (2006), Snowpack variations in the central Andes of Argentina and Chile, 1951–2005: Large-scale atmospheric influences and implica-tions for water resources in the region, *J. Clim.*, *19*, 6334–6352, doi:10.1175/JCLI3969.1.

Masiokas, M. H., A. Rivera, L. E. Espizua, R. Villalba, S. Delgado, and J. C. Aravena (2009), Glacier fluctuations in extratropical South America during the past 1000 years, *Palaeogeogr. Palaeoclimatol. Palaeoecol.*, *281*, 242–268, doi:10.1016/j.palaeo.2009.08.006.

Masiokas, M. H., R. Villalba, B. H. Luckman, and S. Mauget (2010), Intra-to multi-decadal variations of snowpack and streamflow records in the Andes of Chile and Argentina between 30° and 37°S, *J. Hydrometeorol.*, *11*(3), 822–831, doi:10.1175/2010JHM1191.1.

Meko, D., C. W. Stockton, and W. R. Boggess (1995), The tree-ring record of severe sustained drought, *Water Resour. Bull.*, *31*(5), 789–801.

Meko, D. M., C.A. Woodhouse, C. H. Baisan, T. Knight, J. J. Lukas, M. K. Hughes, and M. W. Salzer (2007), Medieval drought in the Upper Colorado River Basin, *Geophys. Res. Lett.*, *34*, L10705, doi:10.1029/2007GL029988.

Michaelsen, J. (1987), Cross-validation in statistical climate forecast models, *J. Clim. Appl. Meteorol.*, *26*, 1589–1600, doi:10.1175/1520-0450(1987)026<1589:CVISCF>2.0.CO;2.

Miller, A. (1976), The climate of Chile, in *World Survey of Climatology: Climates of Central and South America*, edited by W. Schwerdtfeger, pp. 113–131, Elsevier, Amsterdam.

Montecinos, A., and P. Aceituno (2003), Seasonality of the ENSO-Related rainfall variability in central Chile and associated circulation anomalies, *J. Clim.*, *16*, 281–296, doi:10.1175/1520-0442(2003)016<0281:SOTERR>2.0.CO;2.

Myers, N., R. A. Mittermeier, C. G. Mittermeier, G. A. da Fonseca, and J. Kent (2000), Biodiversity hotspots for conservation priorities, *Nature*, *403*, 853–858, doi:10.1038/35002501.

NC-Chile (1999), 1st national communication to the UNFCCC, 89 pp., Santiago.

Niemeyer, H., and P. Cereceda (1984), *Colección Geográfica de Chile*, vol. 8, *Hidrografía*, 313 pp., Inst. Geogr. Mil., Santiago.

Olson, D. M., and E. Dinerstein (2002), The Global 200: Priority ecoregions for global conservation, *Ann. Mo. Bot. Gard.*, 89, 199–224, doi:10.2307/3298564.

Osborn, T. J., K. B. Briffa, and P. D. Jones (1997), Adjusting variance for sample size in tree-ring chronologies and other regional mean timeseries, *Dendrochronologia*, 15, 89–99.

Pezoa, L. S. (2003), Recopilación y análisis de la variación de las temperaturas (período 1965–2001) y las precipitaciones (período 1931–2001) a partir de la información de estaciones meteorológicas de Chile entre los 33° y 53° de latitud sur, B.S. thesis, Esc. de Ing. For., Univ. Austral de Chile, Valdivia, Chile.

Philip, S., and G. van Oldenborgh (2006), Shifts in ENSO coupling processes under global warming, *Geophys. Res. Lett.*, 33, L11704, doi:10.1029/2006GL026196.

Quintana, J. M. (2004), Factors affecting central Chile rainfall variations at interdecadal scales [in Spanish], M.Sc. thesis, Univ. de Chile, Santiago.

Rodriguez-Cabal, M. A., M. A. Nuñez, and A. S. Martínez (2008), Quantity versus quality: Endemism and protected areas in the temperate forest of South America, *Austral Ecol.*, 33, 730–736, doi:10.1111/j.1442-9993.2008.01841.x.

Rubio-Álvarez, E., and J. McPhee (2010), Patterns of spatial and temporal variability in streamflow records in south central Chile in the period 1952–2003, *Water Resour. Res.*, 46, W05514, doi:10.1029/2009WR007982.

Rutllant, J., and H. Fuenzalida (1991), Synoptic aspects of the central Chile rainfall variability associated with the Southern Oscillation, *Int. J. Climatol.*, 11, 63–76, doi:10.1002/joc.3370110105.

Schulman, E. (1956), *Dendroclimatic Change in Semiarid America*, Univ. of Ariz. Press, Tucson.

Searcy, J. C. (1959), Flow duration curves, *U.S. Geol. Surv. Water Supply Pap.*, 1542A.

Sheppard, P. R., P. E. Tarasov, L. J. Graumlich, K.-U. Heussner, M. Wagner, H. Österle, and L. G. Thompson (2004), Annual precipitation since 515 BC reconstructed from living and fossil juniper growth of northeastern Qinghai Province, China, *Clim. Dyn.*, 23(7–8), 869–881, doi:10.1007/s00382-004-0473-2.

Shindell, D., and G. Schmidt (2004), Southern Hemisphere climate response to ozone changes and greenhouse gas increases, *Geophys. Res. Lett.*, 31, L18209, doi:10.1029/2004GL020724.

Smith, T. M., and R. W. Reynolds (2003), Extended reconstruction of global sea surface temperatures based on COADS data (1854–1997), *J. Clim.*, 16, 1495–1510, doi:10.1175/1520-0442-16.10.1495.

Stockton, C. W., and G. C. Jacoby (1976), Long-term surface-water supply and streamflow trends in the Upper Colorado River Basin based on tree-ring analyses, *Lake Powell Res. Proj. Bull.*, 1, 1–70.

Thompson, D. W. J., and S. Solomon (2002), Interpretation of recent Southern Hemisphere climate change, *Science*, 296, 895–899, doi:10.1126/science.1069270.

Thompson, D., and J. M. Wallace (2000), Annular modes in the extratropical circulation. Part I: Month-to-month variability, *J. Clim.*, 13, 1000–1016, doi:10.1175/1520-0442(2000)013<1000:AMITEC>2.0.CO;2.

Torrence, C., and G. P. Compo (1998), A practical guide to wavelet analysis, *Bull. Am. Meteorol. Soc.*, 79, 61–78, doi:10.1175/1520-0477(1998)079<0061:APGTWA>2.0.CO;2.

Trenberth, K. E., et al. (2007), Observations: Surface and atmospheric climate change, in *Climate Change 2007: The Physical Science Basis. Contribution of Working Group I to the Fourth Assessment Report of the Intergovernmental Panel on Climate Change*, edited by S. Solomon et al., pp. 235–336, Cambridge Univ. Press, Cambridge, U. K.

van Oldenborgh, G. S. P., and M. Collins (2005), El Niño in a changing climate: A multi-model study, *Ocean Sci.*, 1, 81–95, doi:10.5194/os-1-81-2005.

Vautard, R., and M. Ghil (1989), Singular spectrum analysis in nonlinear dynamics, with applications to paleoclimatic time series, *Physica D*, 35, 395–424, doi:10.1016/0167-2789(89)90077-8.

Vecchi, G. A., and A. T. Wittenberg (2010), El Niño and our future climate: Where do we stand?, *Wiley Interdiscip. Rev. Clim. Change*, 1(2), 260–270.

Villagrán, C., and L. F. Hinojosa (1997), Historia de los bosques del sur de Sudamérica, II: Análisis fitogeográfico, *Rev. Chil. Hist. Nat.*, 70, 241–267.

Villalba, R., J. A. Boninsegna, A. Lara, T. Veblen, F. Roig, J. C. Aravena, and A. Ripalta (1996), Interdecadal climatic variations in millennial temperature reconstructions from southern South America, in *Climatic Variations and Forcing Mechanisms of the Last 2000 Years*, *NATO ASI Ser.*, vol. 141, edited by P. D. Jones, R. S. Bradley, and J. Jouzer, pp. 161–189, Springer, Berlin.

Villalba, R., E. Cook, G. Jacoby, R. D'Arrigo, T. Veblen, and P. Jones (1998), Tree-ring based reconstructions of northern Patagonia precipitation since AD 1600, *Holocene*, 8(6), 659–674, doi:10.1191/095968398669095576.

Visbeck, M. (2009), A station-based Southern Annular Mode index from 1884 to 2005, *J. Clim.*, 22, 940–950, doi:10.1175/2008JCLI2260.1.

Viviroli, D., R. Weingartner, and B. Messerli (2003), Assessing the hydrological significance of the world's mountains, *Mt. Res. Dev.*, 23(1), 32–40, doi:10.1659/0276-4741(2003)023[0032:ATHSOT]2.0.CO;2.

Wigley, T. M., K. R. Briffa, and P. D. Jones (1984), On the average value of correlated time series with applications in dendroclimatology and hydrometeorology, *J. Clim. Appl. Meteorol.*, 23, 201–213, doi:10.1175/1520-0450(1984)023<0201:OTAVOC>2.0.CO;2.

Woodhouse, C. A. (2001), A tree-ring reconstruction of streamflow for the Colorado Front Range, *J. Am. Water Resour. Assoc.*, 37(3), 561–569, doi:10.1111/j.1752-1688.2001.tb05493.x.

Woodhouse, C. A., and J. Lukas (2006), Multi-century tree-ring reconstructions of Colorado streamflow for water resource planning, *Clim. Change*, 78(2–4), 293–315, doi:10.1007/s10584-006-9055-0.

Woodhouse, C. A., S. T. Gray, and D. M. Meko (2006), Updated streamflow reconstructions for the Upper Colorado River Basin, *Water Resour. Res.*, 42, W05415, doi:10.1029/2005WR004455.

D. A. Christie, A. Cuq, A. Lara, and C. Le Quesne, Laboratorio de Dendrocronología, Instituto de Silvicultura, Facultad de Ciencias Forestales y Recursos Naturales, Universidad Austral de Chile, Casilla 567, Valdivia, Chile.

R. B. Urrutia, Environmental Change Institute, School of Geography and the Environment, University of Oxford, South Parks Road, Oxford OX1 3QY, UK. (rocio.urrutia@ouce.ox.ac.uk)

R. Villalba, Departamento de Dendrocronología e Historia Ambiental, Instituto Argentino de Nivología, Glaciología y Ciencias Ambientales, CONICET, C.C. 330, 5500 Mendoza, Argentina.